https://doi.org/10.5194/egusphere-2024-744
Preprint. Discussion started: 3 April 2024

Monitoring snow depth variations in an avalanche release area using low cost LiDAR and optical sensors

Pia Ruttner-Jansen[1,2,3], Annelies Voordendag[3], Thierry Hartmann[1], Julia Glaus[1,2,4], Andreas Wieser[3], and Yves Bühler[1,2]

[1]WSL Institute for Snow and Avalanche Research SLF, Davos Dorf, 7260, Switzerland
[2]Climate Change, Extremes, and Natural Hazards in Alpine Regions Research Center CERC, Davos Dorf, 7260, Switzerland
[3]Institute of Geodesy and Photogrammetry, ETH Zurich, Zurich, 8092, Switzerland
[4]Institute for Geotechnical Engineering, ETH Zurich, Zurich, 8092, Switzerland

Correspondence: Pia Ruttner-Jansen (pia.ruttner@slf.ch)

Abstract. Snow avalanches threaten people and infrastructure in mountainous areas. For the assessment of temporal protection measures of infrastructure in dangerous situations, local and up to date information is crucial. One factor influencing the avalanche situation is wind drifted snow, which causes variations in snow depth across a slope, but this data is rarely available. We present a monitoring system using low cost LiDAR and optical sensors, which we use to monitor snow depth variations in an avalanche release area. The system is operational since November 2023, autonomously measuring and providing data from our study area close to Davos in Switzerland, with high spatiotemporal resolution. In the first three operating months we gained experiences and made a preliminary assessment of the system performance. An analysis of the changes in spatial coverage shows the limitations and potentials of the system under different weather conditions. A comparison of ~~the~~ surface models derived from the LiDAR data and a photogrammetric drone shows ~~a~~ good agreement, achieving a mean of 0.005 m and standard deviation of 0.15 m. Two case studies, including an avalanche event and a period of snowfall with strong winds, show the potential of the proposed system to detect changes in the snow depth distribution on a low decimeter level, or better. In addition, we record meteorological parameters which we will use in future, together with the newly established snow depth database, for attempts to refine and further develop models for wind-induced snow redistribution. The near real time information of the snow depth distribution in avalanche prone slopes will be provided to experts, so it can aid their decisions on avalanche safety measures.

1 Introduction

People and infrastructure in mountainous areas with seasonal snow cover face the danger of avalanches. There are different possibilities to mitigate the associated risks. ~~Among other measures,~~ in some cases traffic routes have to be completely closed ~~in dangerous situations~~. Such a closure has a significant impact on people and the economy, so the aim is to keep the period of closure as short as possible. However, the local experts have in most cases limited information on which to base their decision. They mainly rely on the avalanche bulletin, the weather forecast, if available automated weather stations, and most importantly, on their own intuition and experience. Among other parameters, the current snow depth distribution in the avalanche release ar-

https://doi.org/10.5194/egusphere-2024-744
Preprint. Discussion started: 3 April 2024

eas would be valuable information. The variations in snow depth provide information about the proportion of snow transported by the wind, which is one of the major drivers causing avalanches (Schweizer et al., 2003).

There are different possibilities of measuring snow depths. The most traditional method is to stick a pole or stake with a scale into the snow cover and read off the snow depth, which gives a point measurement at a specific time. This type of measurements can also provide a time series, if the pole is permanently installed and a camera is set up to automatically take pictures of the pole (Garvelmann et al., 2013; Dong and Menzel, 2017; Kopp et al., 2019). Other methods for the measurement of snow depth as a time series are the use of ultrasonic sensors, often as part of automatic weather stations (Lehning et al., 1999), or GNSS reflectometry (Larson et al., 2009). However, single point measurements give only local information and do not reveal the variations of snow depth across a slope.

For areal acquisitions of the snow cover the most used systems are LiDAR (Light Detection and Ranging) sensors and photo cameras. Both systems are either used from the air or on the ground. Airborne systems have the advantage of better spatial coverage (less topographic occlusions) and optimal acquisition angles (sensors on the platform approximately looking downward have an (mostly) orthogonal view on the recorded surface). Civilian Uncrewed Aerial Vehicles (UAVs) typically operate at low altitudes above ground (e.g., up to about 200 m). When used as a carrier platform for photo cameras or LiDAR sensors, they therefore allow obtaining a high spatial resolution (cm-level) (Bühler et al., 2016; Harder et al., 2016; Jacobs et al., 2021), but the area that can be covered per campaign is limited to a few square kilometers. When using airplanes (Bühler et al., 2015; Nolan et al., 2015; Bührle et al., 2023) or satellite platforms (Romanov et al., 2003; Marti et al., 2016; Shaw et al., 2020), the covered area can be much bigger, but the achievable spatial resolution decreases.

However, when using airborne systems, the temporal resolution is usually limited. With a ground based system, that can measure (almost) continuously and autonomously, an area of interest can be acquired with higher temporal resolution, but with the drawback of having shadowing effects due to topography and often unfavourable acquisition angles (large angles between the sensor and the surface normal).

For the computation of a 3D model using photo cameras, each point needs to be captured in at least two images from different viewpoints. This can be achieved with a setup of multiple cameras (Basnet et al., 2016; Deschamps-Berger et al., 2020; Filhol et al., 2019; Mallalieu et al., 2017) or one moving camera capturing overlapping images, (Liu et al., 2021; Bühler et al., 2015; Bührle et al., 2023; Marti et al., 2016; Shaw et al., 2020). Photogrammetric approaches rely on recognisable features in the acquired images. For the application on snow it is important that the snow cover shows certain features, for example structures induced by the wind, and that the light conditions are favourable, such that those features are visible in the captured images (Bühler et al., 2016, 2017).

LiDAR sensors on the other hand use an active measurement technique, where modulated light is emitted, e.g., a light pulse, the direction of emission and the time of flight until reception of the reflected light are recorded, and the position of the reflecting surface relative to the LiDAR sensor is calculated. Therefore, compared to photogrammetric acquisitions, LiDAR sensors are less dependent on the ambient light, do not require radiometric surface texture, and can also measure during the night. An important criterion for the application of LiDAR sensors on snow is the operating wavelength. The most suitable wavelengths are in the near infrared (Wiscombe and Warren, 1980; Prokop, 2008). Most available LiDAR sensors use a wavelength of 1550

https://doi.org/10.5194/egusphere-2024-744
Preprint. Discussion started: 3 April 2024

nm, where the reflectance of snow has a local minimum. It is possible to measure snow at that wavelength, but the achievable range is constrained (with respect to the maximum range specification of the sensor), and the snow surface needs to be dry and compact. The highest reflectance of snow is at around 500 nm, but at this wavelength the penetration of the signal into the snowpack reaches about 10 cm (Deems et al., 2013), so the reflected signal does not represent only the snow surface. The optimal wavelengths are at 900-1100 nm, where the reflectance of snow is high, and the majority of the signal is reflected from the top 1 cm (Deems et al., 2013). The best known LiDAR sensor for the application on snow and ice is the Riegl VZ6000 terrestrial laser scanner (TLS), which was especially developed for that purpose. It uses a wavelength of 1064 nm and has a measurement range of up to 6000 m. It is used in various applications, often to measure glaciers at large scale (Voordendag et al., 2021; LeWinter et al., 2014), or studies to monitor snow surface variations (Hancock et al., 2018; Fey et al., 2019). However, the Riegl VZ6000 TLS is very costly (>200k USD), its operation at short ranges (few hundred meters) is not eye safe and an autonomous operation is complex, in terms of power supply, a stable setup of the sensor and weather protection (Voordendag et al., 2023).

Alternatives can be found in the automotive industry, where the market for low-cost LiDAR sensors is evolving fast. Many of these sensors have a wavelength of around 900 nm, they are very robust for harsh environments as they are designed for year-round outdoor use, and they operate in the short to medium range (maximum few hundred metres). In geomonitoring applications these LiDAR sensors are often used on UAVs (Jacobs et al., 2021; Hu et al., 2021), or on ground-based platforms (Jaakkola et al., 2014; Bakuła et al., 2022).

Herein we propose a monitoring system, that is using a low cost LiDAR sensor in a static ground-based, ~~and~~ automatic and autonomous application. The aim is to monitor the snow depth variations in an avalanche release area at high spatiotemporal resolution. In this paper we present the monitoring system and the experiences over the first three operating months. We also present preliminary results and case studies, that show the potentials and limitations of the proposed system.

2 Monitoring System

The purpose of the monitoring system is to build up a snow depth database of high spatial and temporal resolution covering an avalanche release area. The main snow depth measurements are done using LiDAR sensors. RGB images collected using SLR cameras complement these data. Additionally, we record meteorological parameters (wind speed and direction, air temperature, relative humidity, and snow surface temperature), which will later serve as basic data for a modelling approach, where we aim to predict the snow depth variations. The system is ground-based, operates autonomously (power supply by solar panel and wind turbine) and transfers the data regularly to a server (once per hour). In the remainder of this section, we elaborate on the chosen instruments, power supply, local storage and data transmission.

https://doi.org/10.5194/egusphere-2024-744
Preprint. Discussion started: 3 April 2024

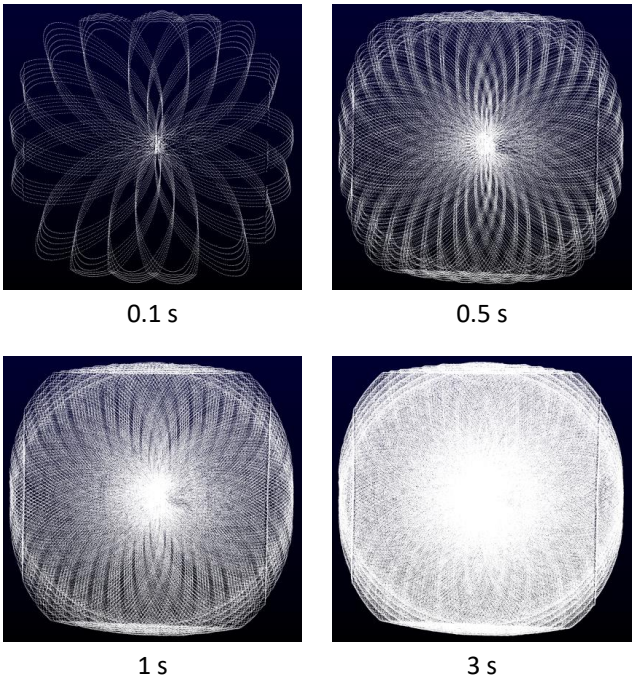

Figure 1. Scanning pattern of the Livox Avia LiDAR sensor in an indoor test setting; spatial coverage increases with scanning time (the flattening on top and bottom, and the linear features on the sides are related to the shape of the room).

2.1 Instrumentation

2.1.1 LiDAR

The most important criteria for the LiDAR sensor in our application are the operating wavelength, maximum range, suitability for outdoor use, and cost. In the fast evolving market of low-cost LiDAR sensors, most of the devices are solid-state sensors, operating with a fixed number of scan lines, usually 32, 64 or 128 (Altuntas, 2022). In a mobile application the spatial coverage increases with the movement of the sensor, but in a static setup the fixed angular spacing between the scan lines of solid-state sensors results in relatively sparse coverage of the scanned scene.

Based on a market survey of LiDAR sensors and their technical specifications, we selected the Livox Avia LiDAR sensor for our measurement system. This sensor uses a Risley prism-based non-repetitive scanning pattern (Vuthea and Toshiyoshi, 2018) instead of fixed scan lines. This allows for a successively denser spatial coverage with increasing scanning times, also when not moving the sensor itself (figure 1). Furthermore, the selected sensor operates at a wavelength of 905 nm, has laser class 1 (i.e., it is eye-safe), has a maximum detection range of 450 m, a power consumption of 8 W and costs less than 2k USD. Further specifications, compared to similar LiDAR sensors on the market, are listed in table 1.

https://doi.org/10.5194/egusphere-2024-744
Preprint. Discussion started: 3 April 2024

Table 1. Specifications of selected LiDAR sensors. Values that are not published by the manufacturer are denoted with "-".

Specification	Livox Avia	Hesai Pandar128	Ouster OS2	Quanenergy M8 Prime Ultra	Velodyne Alpha Prime
Wavelength [nm]	905	905	865	905	903
Max. range [m]	450	200	350	200	300
Field of View (HxV)	70.4° x 77.2°	360° x 40°	360° x 22.5°	360° x 20°	360° x 40 °
Range Accuracy	-	2-10 cm (1-200 m)	5 cm	3 cm (1σ @ 50m)	3 cm
Range Precision	2 cm (1σ @ 20m)	-	2-10 cm	-	-
Angular Precision (1σ)	<0.05°	-	0.01°	-	-
Beam Divergence	0.28° × 0.03° (VxH)	-	0.09° (FWHM)	-	-

Figure 2. Example images of camera at station Braema1 (see figure 3) on January 31, 2024, at midnight (00:00 UTC) and in the morning (08:00 UTC). The distance to station Braema2 on the ridge is about 160 m.

2.1.2 Camera

A camera provides visual information about the conditions and processes in the release zone, such as weather conditions, or traces of avalanche events, animals and sportspersons. We chose a Canon EOS R7 32 megapixel camera with an RF-S 18-45 mm F4.5-6.3 IS STM zoom lens. This allows an on site adjustment for capturing roughly the same area with the camera and the LiDAR sensor. The camera operates in aperture-value (Av) mode, with the aperture set to f/8. The shutter speed is automatically adjusted by the camera for optimal exposure. This allows for acquisitions at day and—during periods with sufficiently strong moon light—at night (figure 2).

2.1.3 Meteorological Sensors

We also installed various meteorological sensors. We record the wind speed and direction using a Young Wind Monitor 05103-L, the relative humidity and air temperature using a Campbell HygroVUE10, and the temperature of the snow surface using a Waljag SnowSurfSDI sensor. Additionally, we measure the temperature in the snowpack, in the vicinity of station Braema2, at

https://doi.org/10.5194/egusphere-2024-744
Preprint. Discussion started: 3 April 2024

the same height and exposition as the avalanche release area. To do this we installed three poles with different height (40, 60 and 80 cm above ground) next to each other, each equipped with a GeoPrecision M-Log 5W temperature sensor on top.

2.1.4 Power and Communication

The measurement stations are designed to operate autonomously. Therefore, they are equipped with a solar panel ($0.69\,\mathrm{m}^2$), and additionally with a wind generator (Phaesun Stormy Wings 400W) for times when the station does not get enough sunlight. The data collected on-site are regularly transmitted to a server so they can be analysed in (near) real time. This makes it possible to recognise malfunctions at an early stage. The remote connection and control are particularly important, as it would be dangerous to access the measurement stations during the winter months.

2.2 Setup and Configuration

2.2.1 Study Site and Setup

The study site is the release area of the "Wildi" avalanche in the Dischma valley, a high alpine valley in the area of Davos in southeast Switzerland (Figure 3). The valley is permanently inhabited, and the road is kept open in winter. Several avalanche paths threaten the road, and it had to be temporarily closed several times in the past years due to avalanche danger (Zweifel et al., 2019). The slope of the study site faces northeast and has an inclination of 30–45 degrees. Figure 3 shows an overview with the mapped outlines of the Wildi avalanche from 2019, as an example of a recent large avalanche in this area. For a suitable coverage of the region of interest we installed two stations (see figure 4). Their locations were determined in three steps: 1) checking the geometrically possible maximum view-shed in a GIS tool, 2) checking the typical snow depths using previous snow depth acquisitions of the area, 3) checking the surroundings of possible locations in the field to find suitable mounting possibilities.

Station Braema1 (figure 5a) is mounted on the side of a large rock in the middle of the slope, on a subtle ridge at an altitude of 2191 m, where the ~~the~~ snow depths are lower than the average of the area, as the snow tends to be eroded by the wind~~,~~ at this location. Station Braema2 (figure 5b) is located on the top of the main ridge (altitude: 2255 m), just high enough to get more sun, but low enough to be able to view into the region of interest. The pole carrying all equipment is screwed directly to the rock on the ground, at this location. Both stations were installed on November 23, 2023.

In order to register the point clouds between epochs identifiable targets in each scan are required. For this purpose we mounted several mini-prisms in the region of interest, choosing places that are assumed to be stable and that are not completely covered in snow in the winter season. However, there were no suitable locations in the slope to be seen from the upper station (Braema2). Looking from top down, everything will be snow covered during the winter season. Therefore, we configured the viewing angle of the upper LiDAR sensor such that its point cloud has a maximum possible overlap with the point cloud from the lower sensor (Braema1). This gives the possibility to register the scans within each epoch directly usingthe point clouds from the two stations, and register them between the epochs by georeferencing using the prisms.

https://doi.org/10.5194/egusphere-2024-744
Preprint. Discussion started: 3 April 2024

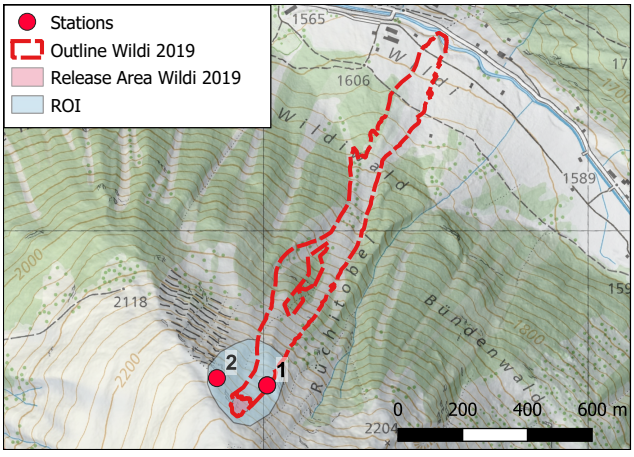

Figure 3. Map of the study area in Dischma valley, with the outline and release area of the Wildi avalanche in 2019, the region of interest (ROI) around the typical release area, and the location of the measurement stations Braema1 (1) and Braema2 (2) (map source: Federal Office of Topography).

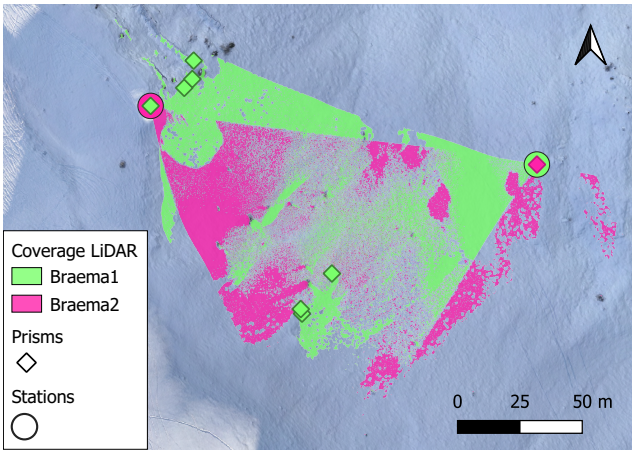

Figure 4. Map of the study area, with the spatial coverage of the two LiDAR sensors, the measurement stations and the prism locations. The color of the prisms indicates which prism is visible from which station. The coverage of the stations is derived from the acquisition of December 23, 2023. The background image is derived from UAV data from December 19, 2023.

For the purpose of potentially later relating the point clouds or the derived results to a superordinate coordinate system (e.g., the Swiss national system LV95), we measured the prism centers using a TCR1203 total station and connected these measruements to a local network of benchmarks, which had in turn been measured using a Trimble RTK-GNSS unit.

https://doi.org/10.5194/egusphere-2024-744
Preprint. Discussion started: 3 April 2024

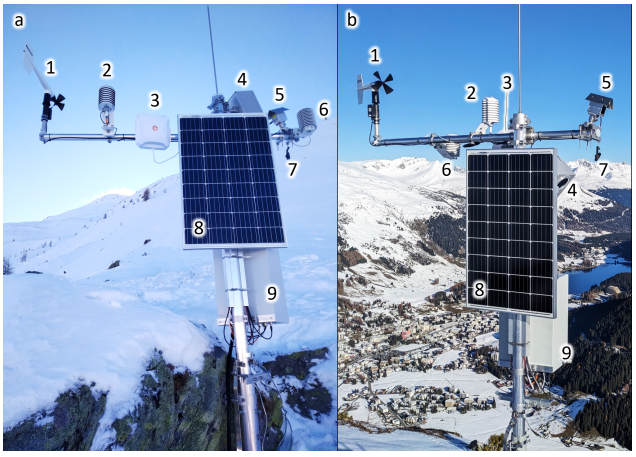

Figure 5. Station Braema1 (a) and Braema2 (b) with 1) anemometer (wind speed and direction), 2) HygroVUE10 (air temperature and relative humidity), 3) communication antenna, 4) camera system, 5) Livox Avia, 6) SnowSurf (snow surface temperature), 7) prism, 8) solar panel, 9) control box (photo: Pia Ruttner-Jansen).

2.2.2 Measurement Configuration

Figure 6 shows a schematic view of all sensors and connections. The measurement system is configured, such that it uses a minimal amount of energy. This means that most instruments and sensors are turned off most of the time, except for the meteorological sensors which need very little energy, and the datalogger, which controls all measurements and data transfers. The data from the meteorological sensors are captured and locally stored by the datalogger every 30 min. At a specified time interval (once per hour) the datalogger supplies a Raspberry Pi computer, a mobile router and the Livox Converter with power for 15 min. As soon as the Rasperry Pi is powered on, it tries to establish a connection with the LiDAR sensor through the mobile router and the Livox Converter. In case of successful communication, the Raspberry Pi triggers a LiDAR measurement which takes 5 s. The scan data are then stored on the local SSD of the Raspberry Pi. If the Raspberry Pi is not able to connect with the Livox Avia sensor within 120 s, it sends an error message to the technical support. After a successful measurement the Raspberry Pi sets the Livox sensor to power-saving mode, and sends the data from the local SSD to a remote server via mobile router and 5G antenna . During the time the router is switched on, the server also retrieves the meteorological measurement data from the logger. The operation of the camera works independently. The photos are triggered at the same time as the LiDAR measurements and are immediately transmitted to the remote server through the 5G antenna.

3 Data Processing

The point clouds of the Livox Avia sensors are first converted from the sensor's binary LVX format to the standard LAS format using a Python script. Afterwards, the point cloud from station Braema2 is transformed to the local system of the point cloud from station Braema1 using the Open3D data processing library (Zhou et al., 2018) implementation of the Iterative Closest

https://doi.org/10.5194/egusphere-2024-744
Preprint. Discussion started: 3 April 2024

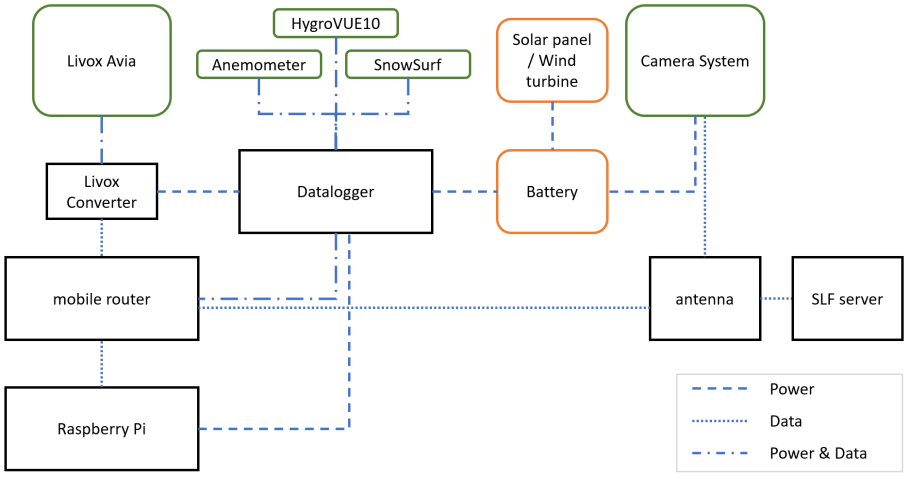

Figure 6. Schematic view of all sensors and connections. Sensors are in green boxes, power related components in orange boxes and all communication modules in black boxes. Dashed lines indicate power connections, dotted lines data communication and the combination of both, indicates a combined connection (power and data).

Point (ICP) plane-to-plane algorithm (Chen and Medioni, 1992). In order to register the different scan epochs with each other, and georeference them to a global coordinate system, we use the prisms, which are installed in the area of interest (see figure 4).

For the computation of snow depth changes we create a gridded digital surface model (DSM), where we project the 3D point clouds along the vertical direction, using the open source software CloudCompare. We define the grid with a cell size of 0.1x0.1 m, which is the average resolution of the point cloud. The cell height is the average of all points within the same grid cell. Empty cells are filled with the linearly interpolated height value from the nearest neighboring cells that are not empty. This is based on Delaunay triangulation, where we define the maximum edge length with 1 m. Empty cells beyond the maximum edge length are filled with the empty cell value "-999". For the analysis of the temporal variations of the spatial coverage of our ROI we define a horizontal 1x1 m^2 grid, counting each grid cell as covered if there is at least 1 scan point with horizontal coordinates within that cell. We then quantify the coverage as percentage of the covered cells among the entire grid (red outline in figure 7, approx. 14'500 m^2).

4 Results

In this section we present preliminary results derived from the data acquired during the first three months of operation, i.e., until February 2024. So far, we have investigated the relation between the meteorological parameters and the coverage of the region of interest (Sect. 4.1), carried out a first comparison of the snow surface obtained from our system and from photogrammetric

https://doi.org/10.5194/egusphere-2024-744
Preprint. Discussion started: 3 April 2024

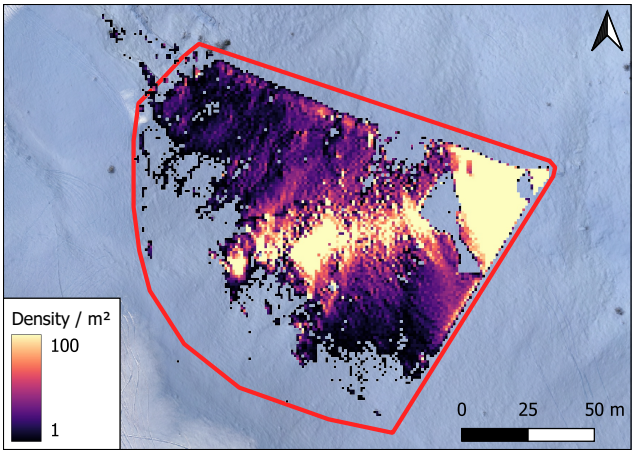

Figure 7. Point cloud from station Braema1 (November 24, 2023, 12:00 UTC) on a 1 m grid, with a customized region of interest (red line), to calculate relative changes of spatial coverage. The grid cells are colored by their point density per m^2. The background image is derived from UAV data from December 19, 2023.

processing of data provided by a start-of-the-art drone (Sect. 4.2), and performed two case studies showing an avalanche event and a snowfall event, respectively, (Sect. 4.3).

4.1 Spatial coverage of region of interest

The maximum spatial coverage of the area of interest depends on the sensor specifications (e.g., the measurement range), the number, spatial distribution and orientation of the LiDAR sensors, on the angle-of-incidence of the laser beams, and on shadowing effects due to the topography. As an example, Figure 4 shows the spatial coverage of the setup at our study site (including both stations) on December 23, 2023, 16:00 UTC. However, changes in the meteorological and snow surface conditions affect the spatial coverage. We analyze this in detail for station Braema1. Figure 8b shows the spatial coverage of station Braema1 over time, together with relevant meteorological parameters, namely incoming short wave radiation (ISWR), snow surface temperature (TSS), height of new snow (HN) within 24 hours, and relative humidity (RH). The ISWR data (Fig. 8a, blue line) are from a nearby weather station ("Stillberg"), about 2 km away from Braema1 and with a similar exposition and elevation. The TSS observations are from the instrument at station Braema1 (Fig. 8a, orange bars). The amount of new snow (HN) is taken from the nearby weather station "Weissfluhjoch", about 5.5 km away from Braema1 and at similar elevation (Fig. 8c, blue to pink bars). The relative humidity is measured directly at Braema1 (Fig. 8c, black line).

The maximum spatial coverage of the ROI obtained from Braema1 is about 70% (Fig. 8b), as the surfaces more than 120–150 m away from the station are hardly covered by the LiDAR sensor (Fig. 7). This uncovered area is however mostly covered by Braema2 (see Fig. 4). The spatial coverage decreases during snowfall events and with high relative humidity, and can be as low as 0%. HN in figure 7 is the new snow accumulation in 24 hours, ~~but this does not mean that it has been continuously~~

https://doi.org/10.5194/egusphere-2024-744
Preprint. Discussion started: 3 April 2024

~~snowing.~~ Due to the high temporal resolution a small weather window (e.g. 1 hour of very light or no snowfall) is sufficient to acquire measurements with high spatial coverage.

There are two periods with big data gaps, one in mid-December and one at the beginning of January (Fig. 8b, light yellow bars). A comparison with the camera images shows, that the camera's lens was covered by snow at these times. We conclude that most likely, also the front side of the LiDAR sensor was covered by snow, and the sensor could therefore not scan the area of interest. However, the coverage increases again as soon as the humidity drops. We assume that the drop of humidity indicates the end of the precipitation and that this coincides ~~temporally~~ with the moments when snow accumulated on the sensor's front glass slides off.

A comparison of the spatial coverage with the ISWR, especially during periods without precipitation, shows a clear diurnal pattern. Around the time of the winter solstice there is no direct sunlight in the ROI at any time of the day, and there is no significant difference between coverage at day and at night (e.g. the period after Dec 15th). With the beginning of the year, the ISWR within the ROI increases, and a diurnal pattern of changing spatial coverage with better coverage during the nights becomes apparent. We assumed that the spatial coverage decreases with TSS close to or above 0°C, due to melting which would result in water on the snow surface and thus less returned laser pulses. However, the surface temperatures recorded so far in our study area are mainly below 0°C, and we do not see an obvious relation between TSS and coverage. Thus, we assume that the above relation between ISWR and coverage is due, at least partially, to the impact of light or radiation reflected towards the LiDAR sensors and degrading their performance. This will have to be further clarified by analyzing data obtained during the spring season, with rising air and snow surface temperatures, and possibly with dedicated experiments in summer, when the sensors can be temporarily taken off the poles for maintenance and special investigations.

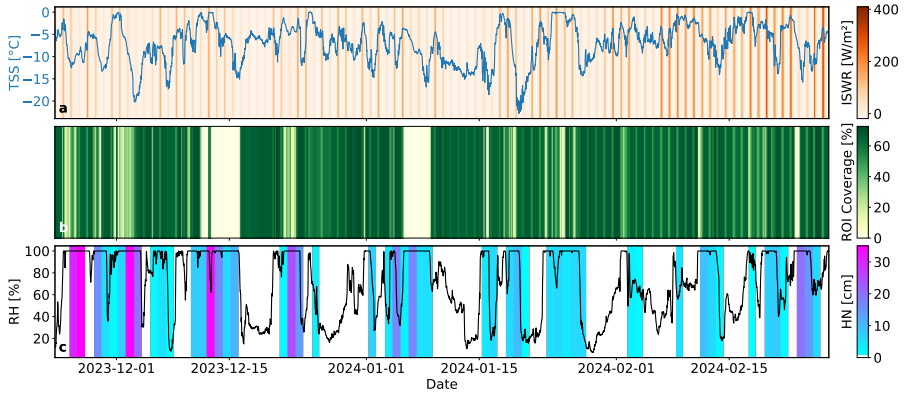

Figure 8. a) Incoming short wave radiation (ISWR, orange bars) and snow surface temperature (TSS, blue line), b) spatial coverage of the ROI (green bars), and c) new snow height (HN, colored bars) and relative humidity (RH, black line).

https://doi.org/10.5194/egusphere-2024-744
Preprint. Discussion started: 3 April 2024

4.2 Comparison with photogrammetric data

We compare the LiDAR point clouds to a photogrammetric UAV acquisition, using a WingtraOne with a 42MP camera. The UAV data was processed similar to Eberhard et al. (2021), resulting in a DSM with 10 cm resolution, achieving about 10 cm vertical accuracy (Bühler et al., 2016). Figure 9 shows the vertical differences between a DSM from a UAV photogrammetric acquisition and the LiDAR point clouds on 19 December 2023. They have a mean of 0.005 m and a standard deviation of 0.15 m. In a direct comparison between the UAV and LiDAR data, the differences strongly depend on the alignment (especially in the vertical direction) of the two DSMs. The differences of the DSMs are larger and noisier at the respective far ends of the LiDAR data. There are also some artefacts which are due to the raw processing status of the LiDAR point cloud. For example at the border of geometrically occluded areas where the angles of incidence are large and the point clouds likely contain mixed pixels (points that are in erroneous locations due to the comparably large LiDAR footprint and the impact of signal back-scattering by objects/surfaces at different distance).

Figure 10 shows the relative differences in snow depth between December 19, 2023 and February 6, 2024 from two photogrammetric UAV acquisitions (Fig. 10b) and, analogously, from the LiDAR point clouds (Fig. 10a) of these two days. The observed snow depth changes from the LiDAR point clouds range between -1.2 and 0.8 m, which is similar to the observed difference from the photogrammetric data with a range between -1.3 and 1 m. The biggest disagreement between the acquisition methods (up to 20 cm difference) is again visible at the far ranges of the LiDAR system (Fig. 10c), and also where the pattern changes from ablation to accumulation, which can be due to errors in the alignment of the systems. Overall, the results differ by a mean of 0.03 m, and the standard deviation of the differences between the UAV results and the LiDAR results is 0.19 m, see Fig. 10c.

4.3 Case study I: Avalanche event

On December 10, 2023 a little avalanche occurred in the ROI. Figure 11 shows the snow depth changes from before to after this avalanche event. Dark red areas indicate snow erosion and blue areas indicate snow deposition. The release zone, crown (fracture line), and track of the avalanche are well visible and the areas not affected by the avalanche do not show big differences between the consecutive epochs. The crown has a height of approximately 0.2 m and the eroded area has a width and a length of 100 m. Although, the length of the eroded area can only be approximated, since the avalanche path ends outside of the monitored area. The upper part of the release zone is not covered by Braema2, due to the limited field of view, and mostly also not by Braema1, due to its range limitation with the high angles of incidence in that area. The influence of the angle of incidence on the range limitation becomes visible with the appearance of the crown in the second epoch. There were no points recorded in that area before the avalanche, but with the increased incidence angle on the crown we can observe it in the second epoch. This avalanche data, combined with the meteorological observations, is useful for the planned modelling of the avalanches in our project.

https://doi.org/10.5194/egusphere-2024-744
Preprint. Discussion started: 3 April 2024

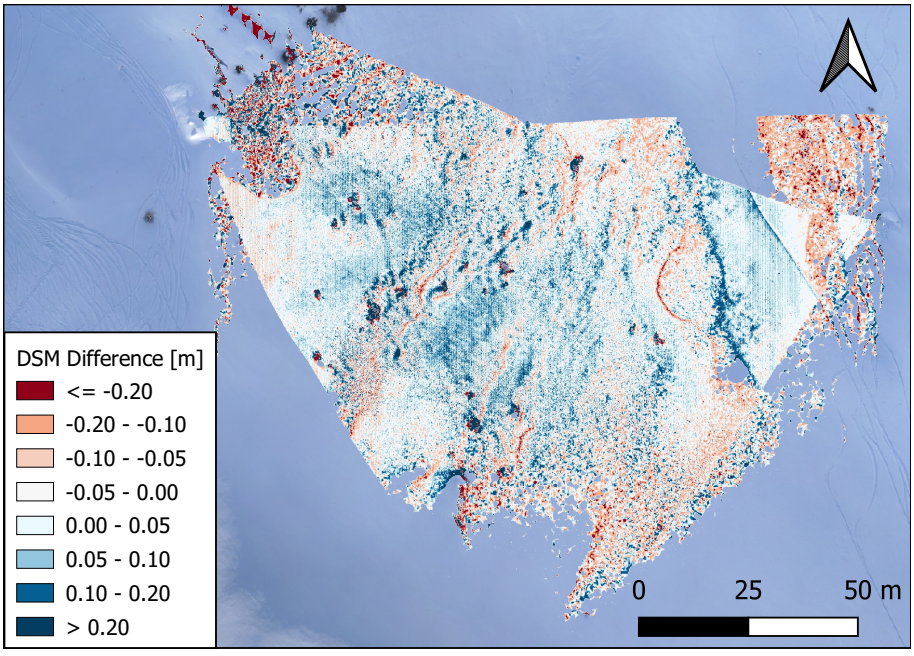

Figure 9. Difference of the DSMs from a UAV photogrammetric acquisition and the LiDAR point clouds on December 19, 2023. The background image is derived from the UAV data.

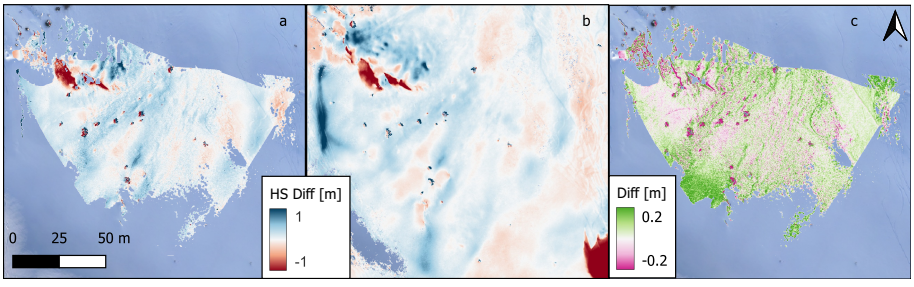

Figure 10. Comparison of the snow depth (HS) differences between December 19, 2023 and February 6, 2024, from a) the LiDAR point clouds and b) photogrammetric UAV acquisitions, and c) shows the difference between a) and b). The background image is derived from UAV data from December 19, 2023.

4.4 Case study II: Snowfall event with wind

Strong winds accompanied by snowfall were observed in the ROI between 22 and 23 December 2023. Figure 12 shows the meteorological conditions around this period, including the wind speed and direction from station Braema2 (30 min average values in blue, and the maximum gusts in orange), and the 24 hour new snow amount from the measurement station at Weissfluhjoch. On December 22, the wind was coming from the west, with an average speed around 25 km/h, and gusts up to 80 km/h. On that day, there were 0.25 m of new snow recorded at Weissfluhjoch. The influence of the strong west-wind is

https://doi.org/10.5194/egusphere-2024-744
Preprint. Discussion started: 3 April 2024

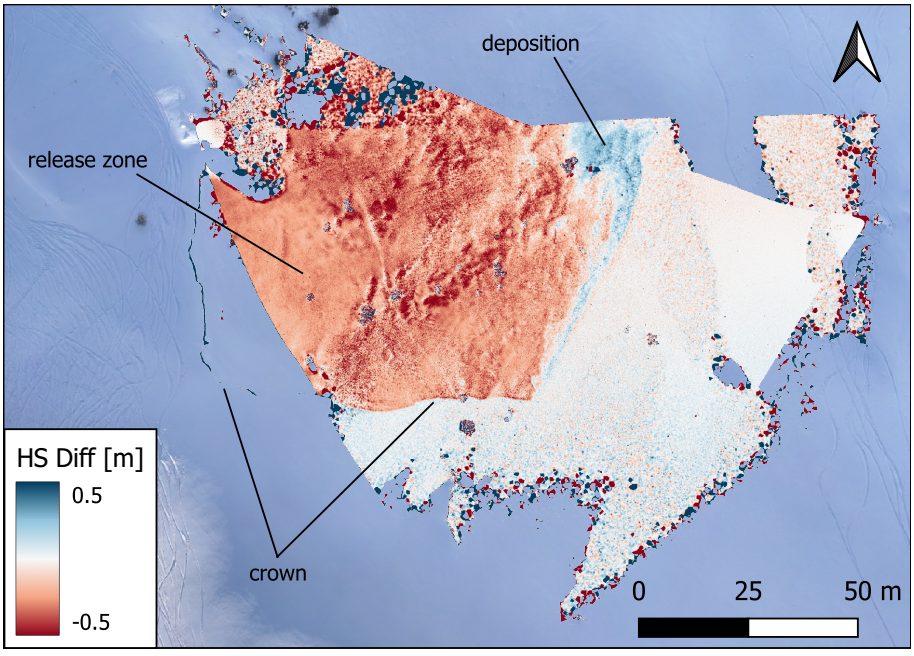

Figure 11. Snow depth (HS) differences derived from LiDAR acquisitions on December 10, 2023 at 11:00 and 12:00 UTC, showing an avalanche event in the ROI. The background image is derived from UAV data from December 19, 2023.

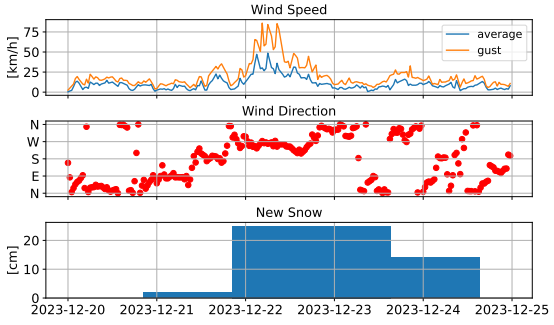

Figure 12. Meteorological conditions (wind speed and direction and amount of new snow) in the ROI in the period of December 20-25, 2023.

clearly visible in the difference of the snow depths from December 21 and 23, 2023 (figure 13). Some areas are eroded (net loss of snow height, despite the snowfall), and to the east of these areas the results indicate a particular increase of the snow height, suggesting additional accumulation related to the wind.

https://doi.org/10.5194/egusphere-2024-744
Preprint. Discussion started: 3 April 2024

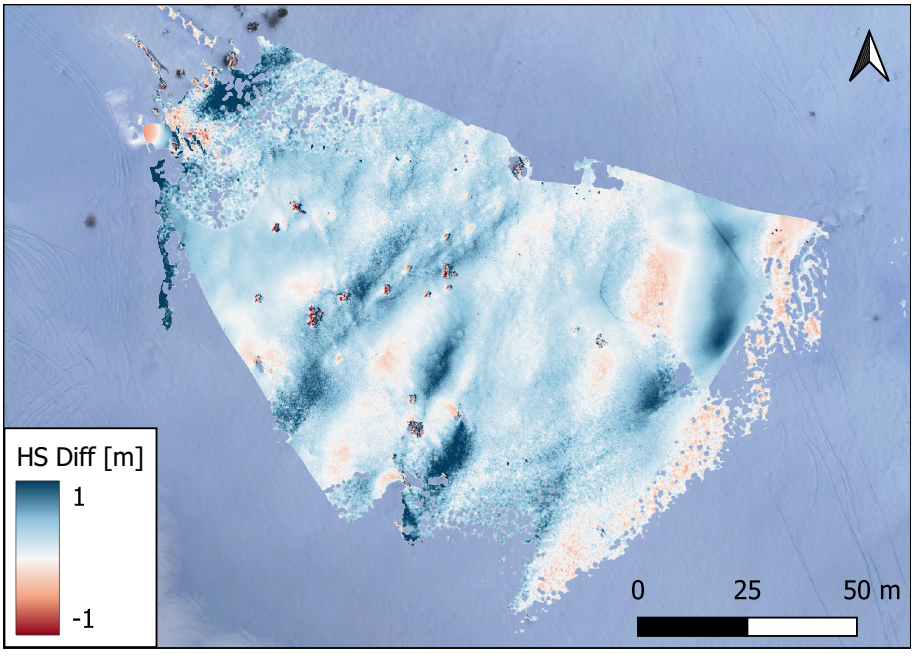

Figure 13. Snow depth (HS) differences derived from LiDAR acquisitions on December 21 (07:00 UTC) and 23 (16:00 UTC), 2023 .

5 Discussion

In comparison with current state of the art methods our system design has a few advantages: The ground-based, autonomous measurements allow for higher temporal resolution than airborne approaches (Bühler et al., 2016; Bührle et al., 2023; Jacobs et al., 2021). The use of the LiDAR sensor enables acquisitions with high spatial resolution at day and night, opposed to purely photogrammetric methods (Basnet et al., 2016; Filhol et al., 2019). Ground-based, autonomously operating LiDAR sensors have been installed before, but at significant higher costs and effort, in terms of sensor protection, stability and power supply (Voordendag et al., 2021). When selecting the sensors for our system, we therefore explicitly focused on outdoor suitability, low weight, low power consumption and overall, low price.

The first three operating months give valuable insights into the potentials and limitations of the ~~proposed~~ monitoring system. While the discrepancies between the UAV-based acquisitions and the early processing results from our system are larger than the expected potential of our system, we consider the agreement an indication that the LiDAR-based system is able to provide snow height differences with high spatial and temporal coverage. The quantification of the currently achieved and achievable accuracy will need further investigations and dedicated experiments, including an assessment of the quality of the photogrammetrically derived snow heights from the UAV as well as the co-registration of UAV and LiDAR results, and the impacts of large angle-of-incidence and mixed pixels in the latter.

The two presented case studies show the potential of the proposed system, where small scale snow depth variations can be detected and also an avalanche is clearly visible in the data. In the case of an avalanche event the high temporal resolution

https://doi.org/10.5194/egusphere-2024-744
Preprint. Discussion started: 3 April 2024

enables an acquisition shortly before and after the event. ~~Therefore,~~ the release depth and volume can be directly derived from the measurements, delivering important information for avalanche formation research and simulations.

The system also faces challenges and limitations. A limiting factor for successful acquisitions is the meteorological condition in the ROI. Precipitation and fog strongly limit the possible field of view. The high temporal resolution in our setup enables acquisitions in small weather windows, so we can often obtain a few epochs during periods where other acquisition methods (e.g., UAV flights) would not be feasible.

When transferring the monitoring system to other areas, the biggest challenge is the placement of the stations. There need to be suitable setup possibilities (e.g. large rocks, stable ground), at locations where the geometrically possible view of the system can cover the desired area of interest. For a meaningful comparison between epochs, and with data from other platforms, identifiable and stable targets are needed in the ROI. ~~Tough,~~ these are not always naturally available or the suitable locations where artificial targets can be installed. However, the system itself is designed in such a way that the configuration can be easily adopted. Because it runs autonomously, it can be used in areas that would be too dangerous to carry out manual campaigns and due to it is low-cost, multiple systems can be installed and used simultaneously.

6 Conclusions

The monitoring system proposed herein autonomously captures snow depth variations at high spatial (cm to low decimeter) and temporal (hourly) resolution. We designed two stations~~,~~ that are installed in an avalanche release area close to Davos in Switzerland and are in operation from end of November 2023. With the analysis of the data from the first three operating months we can show the capabilities ~~and limitations of the system~~, to capture snow depth variations relevant for avalanche release estimation. Such information could help in the future to improve safety management at avalanche prone traffic routes.

The analysis of the relative changes of spatial coverage of the region of interest provides an initial indication of the influence of the snow surface and weather conditions on the measurement performance. A comparison of surface models derived from LiDAR and photogrammetric drone data shows a mean height difference of 0.005 m with a standard deviation of 0.15 m, indicating an accuracy of the LiDAR data at a low dm level or better. We achieve a similar agreement between the two systems (LiDAR and photogrammetric drone data) when comparing snow depth changes between acquisitions from December 19, 2023 and February 6, 2024. On December 10, 2023 an avalanche event occurred in the study area, which was well captured by the system, allowing to derive the width of the release zone (about 100 m), as well as the release height (about 0.2 m). In a second case study, we were able to demonstrate the potential for investigating wind-induced snow depth redistribution during a 3-day snowfall event with strong winds.

~~Nevertheless,~~ further processing of the data is needed, including automated procedures for data filtering, smoothing and georeferencing. Future investigations will also include additional comparisons with other sensors (e.g. the Riegl VZ6000 laser scanner and and DJI L2 LiDAR drone) and dedicated experiments (e.g. the effect of light on the sensors) in order to better quantify the performance of the monitoring system.

https://doi.org/10.5194/egusphere-2024-744
Preprint. Discussion started: 3 April 2024

The newly established database will be expanded in the following seasons, including data from additional installations at further avalanche release zones with different expositions. Furthermore, we will use the high spatiotemporal resolution data of snow depth changes, together with the recorded meteorological parameters for the refinement of avalanche simulations, as well as for the validation of existing and the development of new small scale wind drifting snow models. In the future, we want to make all data available to the local hazard experts to support their decisions on temporary avalanche mitigation and safety measures and compare its benefit to their state of the art approaches mainly based on measurements from a few automated weather stations.

Code and data availability. The data and codes applied will be available on ENVIDAT (https://envidat.ch) on the acceptance of this paper.

Author contributions. Study design: YB, PRJ and JG, Technical implementation: TH, Fieldwork: PRJ, JG, and TH, Data processing: PRJ, with inputs from AV, AW and YB, Manuscript: PRJ with contributions from all co-authors.

Competing interests. At least one of the (co-)authors is a member of the editorial board of Natural Hazards and Earth System Sciences.

Acknowledgements. This research is funded by the Swiss National Science Foundation SNSF with the project "Avalanche Safety for Roads" (Nr. 207519). The authors would like to thank the SLF workshop for designing and producing the hardware for the measurement stations, Andreas Stoffel for operating the Wingtra drone and Jor Fergus Dal and Justine Sommerlatt for their support during field work.

https://doi.org/10.5194/egusphere-2024-744
Preprint. Discussion started: 3 April 2024

References

Altuntas, C.: Point Cloud Acquisition Techniques by Using Scanning Lidar for 3d Modelling and Mobile Measurement, The International Archives of Photogrammetry, Remote Sensing and Spatial Information Sciences, XLIII-B2-2022, 967–972, https://doi.org/10.5194/isprs-archives-XLIII-B2-2022-967-2022, num Pages: 967-972 Place: Gottingen, Germany Publisher: Copernicus GmbH, 2022.

Bakuła, K., Lejzerowicz, A., Pilarska-Mazurek, M., Ostrowski, W., Górka, J., Biernat, P., Czernic, P., Załęgowski, K., Kleszczewska, K., Węzka, K., Gąsiewski, M., Dmowski, H., and Styś, N.: Sensor Integration and Application of Low-Sized Mobile Mapping Platform Equipped with Lidar, Gpr and Photogrammetric Sensors, The International Archives of Photogrammetry, Remote Sensing and Spatial Information Sciences, XLIII-B1-2022, 167–172, https://doi.org/10.5194/isprs-archives-XLIII-B1-2022-167-2022, num Pages: 167-172 Place: Gottingen, Germany Publisher: Copernicus GmbH, 2022.

Basnet, K., Muste, M., Constantinescu, G., Ho, H., and Xu, H.: Close range photogrammetry for dynamically tracking drifted snow deposition, Cold Regions Science and Technology, 121, 141–153, https://doi.org/10.1016/j.coldregions.2015.08.013, 2016.

Bühler, Y., Marty, M., Egli, L., Veitinger, J., Jonas, T., Thee, P., and Ginzler, C.: Snow depth mapping in high-alpine catchments using digital photogrammetry, The Cryosphere, 9, 229–243, https://doi.org/10.5194/tc-9-229-2015, 2015.

Bühler, Y., Adams, M. S., Bösch, R., and Stoffel, A.: Mapping snow depth in alpine terrain with unmanned aerial systems (UASs): potential and limitations, The Cryosphere, 10, 1075–1088, https://doi.org/10.5194/tc-10-1075-2016, 2016.

Bühler, Y., Adams, M. S., Stoffel, A., and Boesch, R.: Photogrammetric reconstruction of homogenous snow surfaces in alpine terrain applying near-infrared UAS imagery, International Journal of Remote Sensing, 38, 3135–3158, https://doi.org/10.1080/01431161.2016.1275060, publisher: Taylor & Francis _eprint: https://doi.org/10.1080/01431161.2016.1275060, 2017.

Bührle, L. J., Marty, M., Eberhard, L. A., Stoffel, A., Hafner, E. D., and Bühler, Y.: Spatially continuous snow depth mapping by aeroplane photogrammetry for annual peak of winter from 2017 to 2021 in open areas, The Cryosphere, 17, 3383–3408, https://doi.org/10.5194/tc-17-3383-2023, publisher: Copernicus GmbH, 2023.

Chen, Y. and Medioni, G.: Object modelling by registration of multiple range images, Image and Vision Computing, 10, 145–155, https://doi.org/10.1016/0262-8856(92)90066-C, 1992.

Deems, J. S., Painter, T. H., and Finnegan, D. C.: Lidar measurement of snow depth: a review, Journal of Glaciology, 59, 467–479, https://doi.org/10.3189/2013JoG12J154, publisher: Cambridge University Press, 2013.

Deschamps-Berger, C., Gascoin, S., Berthier, E., Deems, J., Gutmann, E., Dehecq, A., Shean, D., and Dumont, M.: Snow depth mapping from stereo satellite imagery in mountainous terrain: evaluation using airborne laser-scanning data, The Cryosphere, 14, 2925–2940, https://doi.org/10.5194/tc-14-2925-2020, 2020.

Dong, C. and Menzel, L.: Snow process monitoring in montane forests with time-lapse photography, Hydrological Processes, 31, 2872–2886, https://doi.org/10.1002/hyp.11229, _eprint: https://onlinelibrary.wiley.com/doi/pdf/10.1002/hyp.11229, 2017.

Eberhard, L. A., Sirguey, P., Miller, A., Marty, M., Schindler, K., Stoffel, A., and Bühler, Y.: Intercomparison of photogrammetric platforms for spatially continuous snow depth mapping, The Cryosphere, 15, 69–94, https://doi.org/10.5194/tc-15-69-2021, publisher: Copernicus GmbH, 2021.

Fey, C., Schattan, P., Helfricht, K., and Schöber, J.: A compilation of multitemporal TLS snow depth distribution maps at the Weisssee snow research site (Kaunertal, Austria), Water Resources Research, 55, 5154–5164, https://doi.org/10.1029/2019WR024788, _eprint: https://onlinelibrary.wiley.com/doi/pdf/10.1029/2019WR024788, 2019.

https://doi.org/10.5194/egusphere-2024-744
Preprint. Discussion started: 3 April 2024

Filhol, S., Perret, A., Girod, L., Sutter, G., Schuler, T. V., and Burkhart, J. F.: Time-Lapse Photogrammetry of Distributed Snow Depth During Snowmelt, Water Resources Research, 55, 7916–7926, https://doi.org/10.1029/2018WR024530, _eprint: https://onlinelibrary.wiley.com/doi/pdf/10.1029/2018WR024530, 2019.

Garvelmann, J., Pohl, S., and Weiler, M.: From observation to the quantification of snow processes with a time-lapse camera network, Hydrology and Earth System Sciences, 17, 1415–1429, https://doi.org/10.5194/hess-17-1415-2013, 2013.

Hancock, H., Prokop, A., Eckerstorfer, M., Borstad, C., and Hendrikx, J.: Monitoring cornice dynamics and associated avalanche activity with a terrestrial laser scanner, International Snow Science Workshop Proceedings 2018, Innsbruck, Austria, pp. 323–327, https://arc.lib.montana.edu/snow-science/item.php?id=2544, 2018.

Harder, P., Schirmer, M., Pomeroy, J., and Helgason, W.: Accuracy of snow depth estimation in mountain and prairie environments by an unmanned aerial vehicle, The Cryosphere, 10, 2559–2571, https://doi.org/10.5194/tc-10-2559-2016, 2016.

Hu, T., Sun, X., Su, Y., Guan, H., Sun, Q., Kelly, M., and Guo, Q.: Development and Performance Evaluation of a Very Low-Cost UAV-Lidar System for Forestry Applications, Remote Sensing, 13, 77, https://doi.org/10.3390/rs13010077, number: 1 Publisher: Multidisciplinary Digital Publishing Institute, 2021.

Jaakkola, A., Hyyppä, J., and Puttonen, E.: Measurement of Snow Depth Using a Low-Cost Mobile Laser Scanner, IEEE Geoscience and Remote Sensing Letters, 11, 587–591, https://doi.org/10.1109/LGRS.2013.2271861, conference Name: IEEE Geoscience and Remote Sensing Letters, 2014.

Jacobs, J. M., Hunsaker, A. G., Sullivan, F. B., Palace, M., Burakowski, E. A., Herrick, C., and Cho, E.: Snow depth mapping with unpiloted aerial system lidar observations: a case study in Durham, New Hampshire, United States, The Cryosphere, 15, 1485–1500, https://doi.org/10.5194/tc-15-1485-2021, 2021.

Kopp, M., Tuo, Y., and Disse, M.: Fully automated snow depth measurements from time-lapse images applying a convolutional neural network, Science of The Total Environment, 697, 134 213, https://doi.org/10.1016/j.scitotenv.2019.134213, 2019.

Larson, K. M., Gutmann, E. D., Zavorotny, V. U., Braun, J. J., Williams, M. W., and Nievinski, F. G.: Can we measure snow depth with GPS receivers?, Geophysical Research Letters, 36, https://doi.org/10.1029/2009GL039430, _eprint: https://onlinelibrary.wiley.com/doi/pdf/10.1029/2009GL039430, 2009.

Lehning, M., Bartelt, P., Brown, B., Russi, T., Stöckli, U., and Zimmerli, M.: snowpack model calculations for avalanche warning based upon a new network of weather and snow stations, Cold Regions Science and Technology, 30, 145–157, https://doi.org/10.1016/S0165-232X(99)00022-1, 1999.

LeWinter, A. L., Finnegan, D. C., Hamilton, G. S., Stearns, L. A., and Gadomski, P. J.: Continuous Monitoring of Greenland Outlet Glaciers Using an Autonomous Terrestrial LiDAR Scanning System: Design, Development and Testing at Helheim Glacier, 2014, C31B–0292, https://ui.adsabs.harvard.edu/abs/2014AGUFM.C31B0292L, conference Name: AGU Fall Meeting Abstracts ADS Bibcode: 2014AGUFM.C31B0292L, 2014.

Liu, J., Chen, R., Ding, Y., Han, C., and Ma, S.: Snow process monitoring using time-lapse structure-from-motion photogrammetry with a single camera, Cold Regions Science and Technology, 190, 103 355, https://doi.org/10.1016/j.coldregions.2021.103355, 2021.

Mallalieu, J., Carrivick, J. L., Quincey, D. J., Smith, M. W., and James, W. H. M.: An integrated Structure-from-Motion and time-lapse technique for quantifying ice-margin dynamics, Journal of Glaciology, 63, 937–949, https://doi.org/10.1017/jog.2017.48, publisher: Cambridge University Press, 2017.

Marti, R., Gascoin, S., Berthier, E., de Pinel, M., Houet, T., and Laffly, D.: Mapping snow depth in open alpine terrain from stereo satellite imagery, The Cryosphere, 10, 1361–1380, https://doi.org/10.5194/tc-10-1361-2016, publisher: Copernicus GmbH, 2016.

https://doi.org/10.5194/egusphere-2024-744
Preprint. Discussion started: 3 April 2024

Nolan, M., Larsen, C., and Sturm, M.: Mapping snow depth from manned aircraft on landscape scales at centimeter resolution using structure-from-motion photogrammetry, The Cryosphere, 9, 1445–1463, https://doi.org/10.5194/tc-9-1445-2015, 2015.

Prokop, A.: Assessing the applicability of terrestrial laser scanning for spatial snow depth measurements, Cold Regions Science and Technology, 54, 155–163, https://doi.org/10.1016/j.coldregions.2008.07.002, 2008.

Romanov, P., Tarpley, D., Gutman, G., and Carroll, T.: Mapping and monitoring of the snow cover fraction over North America, Journal of Geophysical Research: Atmospheres, 108, https://doi.org/10.1029/2002JD003142, _eprint: https://onlinelibrary.wiley.com/doi/pdf/10.1029/2002JD003142, 2003.

Schweizer, J., Bruce Jamieson, J., and Schneebeli, M.: Snow avalanche formation, Reviews of Geophysics, 41, https://doi.org/10.1029/2002RG000123, _eprint: https://onlinelibrary.wiley.com/doi/pdf/10.1029/2002RG000123, 2003.

Shaw, T. E., Deschamps-Berger, C., Gascoin, S., and McPhee, J.: Monitoring Spatial and Temporal Differences in Andean Snow Depth Derived From Satellite Tri-Stereo Photogrammetry, Frontiers in Earth Science, 8, https://www.frontiersin.org/articles/10.3389/feart.2020.579142, 2020.

Voordendag, A., Goger, B., Klug, C., Prinz, R., Rutzinger, M., Sauter, T., and Kaser, G.: Uncertainty assessment of a permanent long-range terrestrial laser scanning system for the quantification of snow dynamics on Hintereisferner (Austria), Frontiers in Earth Science, 11, https://www.frontiersin.org/articles/10.3389/feart.2023.1085416, 2023.

Voordendag, A. B., Goger, B., Klug, C., Prinz, R., Rutzinger, M., and Kaser, G.: AUTOMATED AND PERMANENT LONG-RANGE TERRESTRIAL LASER SCANNING IN A HIGH MOUNTAIN ENVIRONMENT: SETUP AND FIRST RESULTS, ISPRS Annals of the Photogrammetry, Remote Sensing and Spatial Information Sciences, V-2-2021, 153–160, https://doi.org/10.5194/isprs-annals-V-2-2021-153-2021, 2021.

Vuthea, V. and Toshiyoshi, H.: A Design of Risley Scanner for LiDAR Applications, in: 2018 International Conference on Optical MEMS and Nanophotonics (OMN), pp. 1–2, https://doi.org/10.1109/OMN.2018.8454641, 2018.

Wiscombe, W. J. and Warren, S. G.: A Model for the Spectral Albedo of Snow. I: Pure Snow, Journal of the Atmospheric Sciences, 37, 2712–2733, https://doi.org/10.1175/1520-0469(1980)037<2712:AMFTSA>2.0.CO;2, publisher: American Meteorological Society Section: Journal of the Atmospheric Sciences, 1980.

Zhou, Q.-Y., Park, J., and Koltun, V.: Open3D: A Modern Library for 3D Data Processing, https://doi.org/10.48550/arXiv.1801.09847, arXiv:1801.09847 [cs], 2018.

Zweifel, B., Lucas, C., Hafner, E., Techel, F., Marty, C., and Stucki, T.: Schnee und Lawinen in den Schweizer Alpen. Hydrologisches Jahr 2018/19, https://www.dora.lib4ri.ch/wsl/islandora/object/wsl%3A22232/, 2019.